

Electronics Letters



AN INTERNATIONAL PUBLICATION

CONTENTS

8th July 1993 Vol. 29 No. 14

pages 1233-1312

ANTENNAS	page	IMAGE PROCESSING	page
Calculation of antenna mutual coupling from far radiated fields L. D. Bamford, P. S. Hall and A. Fray (UK)	1299	Improved handwritten character recognition using second order information from training set Zs. M. Kovács, R. Ragazzoni, R. Rovatti and R. Guerrieri (Italy)	1308
Incompleteness of the periodic moment method R. C. Hansen (USA)	1245	Interpolative three-level block truncation coding algorithm E. Oshri, N. Shelly and H. B. Mitchell (Israel)	1267
Smooth aperture distribution synthesis for shaped beam reflector antennas B. S. Westcott, A. A. Zaporozhets and A. D. Searle (UK)	1275		
		INFORMATION THEORY	
CIRCUIT THEORY & DESIGN		Algorithmic measures for preventing the middleperson attack in identification schemes C. H. Lim and P. J. Lee (Korea)	1281
Ratiometric temperature stable current reference Y. Deval, S. Gervais Ducouret and J. P. Dom (France)	1284		
		INTEGRATED OPTICS	
COMMUNICATIONS & SIGNAL PROCESSING		High frequency saturation measurements of an InGaAs/InP waveguide photodetector A. R. Williams, A. L. Kellner and P. K. L. Yu (USA)	1298
Accurate interpolation via the discrete W transform Zhiwei Wang, J. J. Soltis and W. C. Miller (Canada)	1282		
Bounds and approximations for the bit error probability of convolutional codes A. G. Burr (UK)	1287	LASERS	
Convolved raised-cosine and triangular-cosine (RCTC) modulation and its performance against timing jitter over noisy channels X.-H. Chen (Singapore)	1239	1 W CW diffraction-limited tunable external-cavity semiconductor laser D. Mehuys, D. Welch and D. Scifres (USA)	1254
Multi-T signalling with coded CPFSK modulation J. P. Fonseka (USA)	1278	20 GHz bandwidth 1.5 µm wavelength VUG DFB laser using a zero net strain In_xGa_{1-x}As₃P_{1-y} well active structure grown at constant y C. Kazmierski, A. Ougazzaden, D. Robein, D. Mathoorasing, M. Blez and A. Mircea (France)	1290
Performance of generalised concatenated codes on fading channels S. A. Shavgulidze (Georgia), V. V. Zyablov (Russia), J. Khunjush and K. H. Hofmann (Germany)	1257	All-solid-state diode-pumped modelocked Cr:LiSAF laser P. M. W. French, R. Mellish, J. R. Taylor (UK), P. J. Delfyett and L. T. Florez (USA)	1262
Symbol and carrier phase synchronisation of MT-MFSK symbols M. J. Evans and K. W. Yates (Australia)	1304	Analysis of threshold current density of CdZnSe/ZnSSe strained quantum well lasers M. Kuramoto, T. C. Chong, A. Kikuchi and K. Kishino (Japan)	1260
		Laser gain and current density in a disordered AlGaAs/GaAs quantum well E. H. Li and K. S. Chan (Hong Kong)	1233
COMPUTERS, LOGIC & MEMORIES		Long wavelength strained-layer InAs/GalnAs single-quantum-well laser grown by molecular beam epitaxy on InP substrate E. Tournié (Germany), P. Grunberg, C. Fouillat, S. Kadret, G. Boissier, A. Baranov, A. Joullié, E. Gaumont-Goarin (France) and K. H. Ploog (Germany)	1255
Fast skew number computation using a CAM and related hardware for an n-bit context predictor G. A. Betzos and J. V. Oldfield (USA)	1265	Low coherence reflectometry using wavelength-tunable superfluorescent fibre source K. Takada and M. Horiguchi (Japan)	1273
ELECTROMAGNETIC WAVES			
Novel basis function for the equivalent magnetic current in the method of moments solution of dielectric scattering problems U. Jakobus and F. M. Landstorfer (Germany)	1272		
FILTERS			
Novel method for designing digital allpass filters based on eigenvalue problem X. Zhang and H. Iwakura (Japan)	1279		

(continued on back cover)

The second term in eqn. 5 determines the number of possible values for m . From eqn. 3 the number of possible values which exist for $(k_{i+1} - k_i)$ is

$$= \frac{2\pi}{\left(\frac{2\pi}{s_i}\right)} = s_i \quad (6)$$

Therefore, there are s_i possible values for m . Now because

$$\begin{aligned} \theta_j + 2\pi k_j &= mn_j + b \\ b &= (\theta_j - mn_j) + 2\pi k_j \end{aligned} \quad (7)$$

and from eqn. 4 there is only one solution for b for each value of m . Therefore, there are s_i lines which fit points from the two sets $(n_i, \theta_i + 2\pi k_i)$ and $(n_{i+1}, \theta_{i+1} + 2\pi k_{i+1})$. ■

Choosing the preamble comb: In an MT-MFSK system (where there is only a single user) there will be at least one comb (with a minimum harmonic spacing of one) available for use by the preamble symbol. In a frequency comb multiple access (FCMA) system [3] there are multiple users using MT-MFSK. In this case, there may not be adequate numbers of combs (with minimum spacing of one) available. The next best choice is to choose combs which have a minimum harmonic spacing of two. The choice of the preamble comb must ensure that there is only one correct line which fits all phase points. This can be achieved by ensuring that the set of comb spacings is relatively prime.

Proof: Given there exists one line which passes through one point from each of the w sets of points, then

$$m = \frac{(\theta_{i+1} - \theta_i)}{p_i c} + \frac{2\pi(k_{i+1} - k_i)}{p_i c} \quad (\text{for all } i) \quad (8)$$

where p_i and c are positive integers and p_i is relatively prime.

From eqns. 3 and 6 the number of possible values which exist for $(k_{i+1} - k_i)$ is $p_i c$. Therefore, for each value of i , the possible values for m are spaced $2\pi/p_i c$ apart.

Given that there is at least one solution for m in eqn. 8, and if there is a common multiple in $p_i c$ for all i , the number of solutions for m will equal this common multiple because the values for m are spaced $2\pi/p_i c$ apart (Fig. 2). Because p_i for all i are relatively prime the common multiple is c . Therefore, there are c solutions for m in $\theta = mn + b$. Using eqn. 7, there are therefore c lines which fit points from all w sets. ■

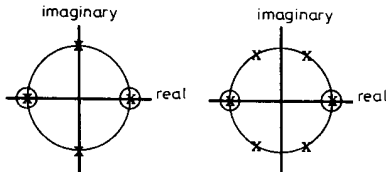


Fig. 2 Example showing that the possible values for slope (m) are 0 and π given the preamble comb: 2, 6, 12 (with a common multiple of $c = 2$)

Conclusion: Synchronisation of the symbol timing and carrier phase of MT-MFSK symbols can be achieved by examining the relationship between phase and harmonic number. The best choice for a preamble comb is one which has a minimum harmonic spacing of one.

In an FCMA system, where multiple users need unique preamble symbols, the set of comb spacings should be relatively prime, and the minimum spacing as low as possible.

These recommendations minimise processing and eliminate ambiguity in the absence of noise. Additional conditions, based on minimising noise sensitivity, are being investigated.

© IEE 1993

7th June 1993

M. J. Evans and K. W. Yates (School of Electrical Engineering, University of Technology, Sydney, PO Box 123, Broadway NSW 2007, Australia)

ELECTRONICS LETTERS 8th July 1993 Vol. 29 No. 14

References

- 1 ATKIN, G. E., and CORRALES, H. P.: 'An efficient modulation/coding scheme for MFSK systems on bandwidth constrained channels', *IEEE J. Sel. Areas Commun.*, 1989, SAC-7, (9), pp. 1396-1401
- 2 YATES, K. W., STEVENSON, T. J., and WATSON, A. P.: 'Multitone M-ary frequency shift keying viewed as spread spectrum'. *IEEE 2nd Int. Symp. on Spread Spectrum Techniques and Applications*, Yokohama, Japan, 1992, pp. 107-110
- 3 YATES, K. W., STEVENSON, T. J., PERCIVAL, T. M. P., BORELI, R., SIMINGTON, R. A. Z., REISENFELD, S., and KWAN, D. K.: 'A new combined modulation and multiple access scheme for VSATs'. *9th Int. Conf. on Digital Satellite Communications*, Copenhagen, Denmark, 1992, pp. 399-405

REDUCTION OF MEASUREMENT ERROR IN MICROWAVE REFLECTOMETRY BY MINIMUM SENSITIVITY CALIBRATION

J. Ladvánszky, A. Hilt and I. Csonka

Indexing terms: Microwave measurements, Reflectometers

Explicit formulas for the sensitivities of the error corrected reflection coefficient (RC) with respect to the RCs of the calibrating elements, and the invariance of their sum are presented. Under the condition that the sum of the sensitivities is constant, the sum of the absolute values of the sensitivities achieves a global minimum if the measured RC coincides with the altitude centre of the triangle formed by the RCs of the calibrating elements, or with one of the RCs of the calibrating elements. In the examples, 8 dB error reduction was found.

Introduction: The measurement of reflection coefficients (RCs) in the microwave frequency range is usually affected by several types of measurement error. For the most common sources of error, the imperfections of the measurement setup can be represented by a linear two-port connected between the ideal reflectometer and the measured device. This two-port is characterised by three complex numbers called error parameters, at each frequency point. To make error-corrected measurements, the error parameters have to be determined from measurements on special devices whose RCs are assumed to be known. This step is called calibration and the special devices are called calibrating elements.

Precise calibrating elements are usually expensive and their imperfection, i.e. the deviation of their RCs from the assumed values, is also a possible source of measurement inaccuracy. In practice more calibrating elements are available than are needed for calibration. Therefore in this Letter we are interested in the minimisation of the effects of the imperfection of the calibrating elements on the result of the measurement by properly selecting the calibrating elements.

Sensitivity minimisation problem: Error parameters can be eliminated [1] using RCs of the calibrating elements x_i and the corresponding RCs read off the instrument y_i ($i = 1, 2, 3$):

$$\frac{x - x_1}{x - x_2} \frac{x_3 - x_2}{x_3 - x_1} = \frac{y - y_1}{y - y_2} \frac{y_3 - y_2}{y_3 - y_1} \quad (1)$$

Our goal is to minimise the inaccuracy of the measured RC, denoted by $|\Delta x|$, caused by the imperfection of the calibrating elements. Δx can be approximated as follows:

$$\Delta x = \frac{\partial x}{\partial x_1} \Delta x_1 + \frac{\partial x}{\partial x_2} \Delta x_2 + \frac{\partial x}{\partial x_3} \Delta x_3 \quad (2)$$

where higher order terms are neglected. For practical reasons inaccuracies of the different calibrating elements are assumed to be equal: $|\Delta x_1| = |\Delta x_2| = |\Delta x_3|$, thus

$$|\Delta x| \leq \left[\left| \frac{\partial x}{\partial x_1} \right| + \left| \frac{\partial x}{\partial x_2} \right| + \left| \frac{\partial x}{\partial x_3} \right| \right] |\Delta x_1| \quad (3)$$

1305

Consequently, the inaccuracy of the measured RC can be decreased by minimising the sum of the absolute values of the sensitivities:

$$P = |S_1| + |S_2| + |S_3| \quad (4)$$

where the sensitivities are defined as follows [2]:

$$S_1 = \frac{\partial x}{\partial x_1} \quad S_2 = \frac{\partial x}{\partial x_2} \quad \text{and} \quad S_3 = \frac{\partial x}{\partial x_3} \quad (5)$$

After some transformation steps, eqns. 1 and 5 yield

$$S_1 = \frac{x - x_2}{x_1 - x_3} \frac{x - x_3}{x_1 - x_2} \quad S_2 = \frac{x - x_3}{x_1 - x_2} \frac{x - x_1}{x_2 - x_3} \quad (6)$$

$$S_3 = \frac{x - x_1}{x_2 - x_3} \frac{x - x_2}{x_3 - x_1}$$

Three calibrating elements are sufficient for calibration. More than three calibrating elements are available. Therefore a question arises: for a known (estimated) x , how should x_1 , x_2 and x_3 be chosen so as to minimise P in eqn. 4. Sensitivity minimisation in a different problem was solved in Reference 2. To apply the method known from Reference 2, the sum of the sensitivities has to be invariant to the choice of x , x_1 , x_2 and x_3 . Eqn. 6 in fact yields

$$M = S_1 + S_2 + S_3 = +1 \quad (7)$$

Thus P in eqn. 4 is minimised under the invariance condition expressed by eqn. 7, by minimising the Lagrange function L :

$$L = \sum_{i=1}^3 [(\text{Re } S_i)^2 + (\text{Im } S_i)^2]^{1/2} - \lambda_1 \sum_{i=1}^3 (\text{Re } S_i - \text{Re } M) - \lambda_2 \sum_{i=1}^3 (\text{Im } S_i - \text{Im } M) \quad (8)$$

where λ_1 and λ_2 are real numbers. As a result, the minimum of the sum of the absolute values of the sensitivities is

$$P_{\min} = |M| = 1 \quad (9)$$

and this minimum is achieved if the phase values of the sensitivities are equal:

$$\text{arc}(S_1) = \text{arc}(S_2) = \text{arc}(S_3) \quad (10)$$

Eqn. 10 holds in the following cases:

(i) *Case 1:* The measured RC x coincides with the height centre of the triangle formed by the calibrating RCs x_1 , x_2 and x_3 on the complex plane. Obtuse triangles are excluded.

The minimum in eqn. 8 is achieved also if:

(ii) *Case 2:* Either $x_1 = x$ or $x_2 = x$ or $x_3 = x$ is selected.

The minimum expressed by eqn. 9 can be achieved only when the measured device is passive. Now we discuss how to find x_2 and x_3 if x_1 and the estimated value of x are given, and $x_1 \neq x$.

Computer optimisation: Find φ_2 and φ_3 that satisfy the following set of equations:

$$x_2 = \exp(j\varphi_2) \quad x_3 = \exp(j\varphi_3) \quad (11)$$

$$\text{Re} \left(\frac{x - x_1}{x_2 - x_3} \right) = \text{Re} \left(\frac{x - x_2}{x_3 - x_1} \right) = \text{Re} \left(\frac{x - x_3}{x_1 - x_2} \right) = 0 \quad (12)$$

where j denotes $\sqrt{-1}$. Eqn. 11 means that calibrating elements are realised by lossless transmission lines that are open ended or terminated by a short. Eqn. 12 is a consequence of case 1.

Geometrical procedure: A diagram of the geometrical procedure is shown in Fig. 1. We exploit the fact that the cali-

brating RCs are on the unit circle. In Fig. 1a X_1 is also on the circle (RC of a lossless transmission line with lossless

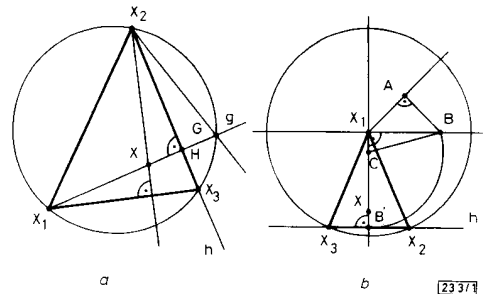


Fig. 1 Diagram of the geometrical procedure that results in two calibrating RCs x_2 and x_3 if the estimated value of the measured RC x and a calibrating RC x_1 are known

- (a) $x_1 = \exp(j\varphi_1)$
(b) $x_1 = 0$

termination). We draw a line g across the points X and X_1 , then find the bisecting point H of the interval GX . We then draw a line h across H so that g and h are perpendicular to each other. The line h intersects the unit circle at the points X_2 and X_3 we are looking for. In Fig. 1b X_1 is the centre of the circle (matched termination). We draw a line g across X_1 that is perpendicular to XX_1 , then draw the isosceles right triangle ABX_1 where $AX_1 = X_1X_2/2$. We then find the quartering point C of the interval XX_1 , and find the point B' on the line XX_1 so that $B'C = BC$. $B'X_1$ is the altitude of triangle $X_1X_2X_3$.

Examples: In the examples the commonly used 50Ω - short - open calibrating set and the optimal one are compared from a sensitivity point of view.

(i) *Example 1:* Let $x = 0.6 + j0.7$, $x_1 = 0$, $x_2 = -1$ and $x_3 = 1$. From eqns. 4-6, $|S_1| = 1.408$, $|S_2| = 0.372$, $|S_3| = 0.805$ and $P = 2.585$ compared to the theoretical minimum expressed by eqn. 8. As a consequence, this set of calibrating elements is a poor choice from a sensitivity point of view.

Now let $x = 0.6 + j0.7$ as above, $\hat{x}_1 = 0$, $\hat{x}_2 = \exp(j1.09)$ and $\hat{x}_3 = \exp(j0.635)$. The phase values have been calculated from eqns. 11 and 12. Now \hat{x}_1 , \hat{x}_2 and \hat{x}_3 form a triangle with centre height x , therefore this is a minimum sensitivity calibrating set. In this case the sensitivities are $|\hat{S}_1| = 0.054$, $|\hat{S}_2| = 0.472$, $|\hat{S}_3| = 0.474$ and $\hat{P} = 1$, that is the theoretical minimum value within the rounding error. The inaccuracy was reduced by $P/\hat{P} = 8$ dB. We note that the last calibrating set can be realised by a 50Ω termination and 50Ω transmission lines terminated by short circuits, at a fixed frequency. This argument shows also the limitation of this method for narrowband measurements.

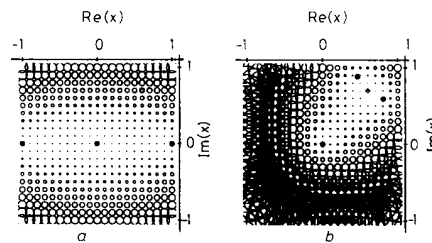


Fig. 2 Sum of absolute value of sensitivities P as function of measured RC x

- calibrating RC
- ◇ measured RC
- (a) 50Ω short - open calibrating set
- (b) Calibrating minimising P in eqn. 4

For comparison, the filled circles correspond to $P = 2.5$; as shown, when the optimum calibrating set is applied, the low-sensitivity area is shifted towards the measured RC

(ii) *Example 2:* To illustrate the sensitivity reduction in example 1 in a more descriptive way, plots of the function $P(x)$ in eqn. 4 are shown in Fig. 2a and b for different calibrating sets. The function $P(x)$ is represented by circles whose centre coincides with the actual value of x , and whose radius is proportional with the corresponding value of $P - P_{min}$. Fig. 2a corresponds to the 50Ω - short - open calibrating set, while our method was applied when Fig. 2b was plotted. Comparison of these Figures shows that low-sensitivity area was shifted towards the measured RC when our method was applied.

Conclusions: In this Letter the measurement error in microwave reflectometers has been reduced by minimising the sum of the absolute values of the sensitivities of the measured RC with respect to the calibrating RCs. The method of sensitivity minimisation by constrained optimisation has been described in detail in Reference 2 where relative and semi-relative sensitivities in lumped element circuits have been considered. Our contribution is the application of the constrained optimisation in microwave measurements based on the invariance of non-relative sensitivities. This Letter also includes our earlier results [3] as a special case. Our method is useful in the case of monolithic microwave and millimetre-wave circuits where fabrication of high-precision calibrating elements is difficult. An extended version of this Letter, including proofs, is available on request.

© IEE 1993

1st June 1993

J. Ladvánszky, A. Hilt and I. Csonka (Research Institute for Telecommunications, H-1525 Budapest, POB 15, Hungary)

References

- 1 BIANCO, B., CORANA, A., RIDELLA, S., and SIMICICH, C.: 'Evaluation of errors in calibration procedures for measurements of reflection coefficient', IEEE Trans., 1978, IM-27, (4), pp. 354-358
- 2 GÉHER, K.: 'Sensitivities of linear networks'. DSc Degree Thesis, Hungarian Academy of Sciences, Budapest, 1972 (in Hungarian)
- 3 LADVÁNSZKY, J., and HILT, A.: 'Minimum sensitivity calibration for reflectometers'. Proc. Int. Workshop on Integrated Nonlinear Microwave and Millimeterwave Circuits, 7-9 October 1992, Duisburg, pp. 153-167

ATTENUATION FUNCTIONS OF MICROWAVE SIGNALS PROPAGATED THROUGH TREES

M. O. Al-Nuaimi and A. M. Hammoudeh

Indexing terms: Microwave measurement, Radiowave propagation

Attenuation of microwave signals at 11.2 GHz through a conifer wood and a regularly planted apple orchard is investigated. The measured attenuation values have been modelled as a function which represents the loss L in dB as $L = kd^m$ where d is the foliage depth in metres and k is a constant.

Propagation measurements were carried out at two test sites under well defined and controlled conditions to measure the propagation loss and attenuation rate through a volume of vegetation at 11.2 GHz. Vegetation attenuation and scatter studies have applications in radio path loss calculations and interference modelling. This includes site shielding where an available vegetation screen may be used to provide protection from unwanted cochannel interference. The first test site in Worcestershire may be referred to as an 'intensive bush cider orchard' which consists of a uniform plantation of apple trees of the same growth with the trees up to 8 m high. Some of the branches have horizontal orientations with respect to the ground surface, others tend to be at angles less than 90° . The branches themselves have spurs, which are evenly spread

along the branches. Leaves start appearing from around the end of May and reach full growth by middle July. The leaves are 5 cm wide and 11 cm long. The initial branching occurs at ~ 1 m from the ground filling the space between columns and rows in all areas. The trees, with a trunk diameter of 25 cm, have a spacing between columns and rows of ~ 2.5 and 6.1 m, respectively. The second site at the Forest of Dean in Gloucestershire is a wedge-shaped mature conifer wood with trees up to 20 m high. Both sites have a clearance in the foreground which was used for installing a transmitter enabling radio-wave illumination of the trees.

The transmitter used in the experiments uses a 25 mW Gunn diode to produce 11.2 GHz CW which is fed to a standard horn antenna with 10 dBi of gain and a 3 dB beamwidth of 53° . The receiver is of a satellite receiving type and employs a low noise block (LNB) to down-convert the received signal to an IF of 1.2 GHz. The receiver employs a 60 cm parabolic dish antenna with 35 dB of gain and a 3 dB beamwidth of 3.2° . The received signal is then displayed on a spectrum analyser which is connected to a portable computer via an IEEE bus to record the signal strength. The receiver noise floor is -75 dBm.

Measurements made using the orchard were conducted with the receiver mounted on a trolley capable of being moved in the restricted space between plantation rows. For each receiver position, the receiving antenna was positioned on a line that passes through a column of trees. The transmitter with its antenna height of 3.5 m above the ground, was fixed on a mast and located at a distance of 200 m from the first line of trees. The incident wave was almost normal to the air-orchard interface. However, measurements on the conifer wood were made with the transmitter at ~ 300 m from the trees and an antenna height of 10 m. The incident wave was at an oblique angle of 60° . The receiver was housed in a vehicle equipped with an extendable mast and a controller, to allow horizontal scanning of the receiving antenna, fixed to its roof.

The measurements at both test sites were made using vertical-vertical polarisation with the receiving antenna at the same height as the transmitting antenna. At each receiver position, the receiving antenna was pointing at the direction of the incident wave. An azimuthal scan of the receiving antenna was performed over an angular range of $\pm 10^\circ$ and the received signal strength was recorded. The highest signal level measured during the azimuthal scan was used for determining the foliage loss.

The attenuation values measured for the conifer wood and the apple orchard with the trees in full leaf are shown in Fig. 1. The measured values are normalised with respect to the

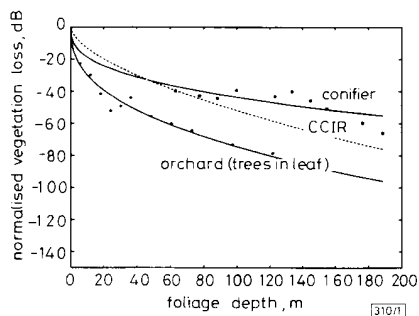


Fig. 1 Measured and modelled foliage loss as a function of foliage depth for conifer wood and orchard (trees in leaf)

signal received at the same point assuming no trees obstructing the path. It is useful in applications and in line with CCIR practice to model the attenuation as a function of the foliage depth. The solid curves are the best fit of the measured points to represent the loss in dB as $L = kd^m$ where d is the foliage depth in metres and k is a constant. It is found that the measured loss can be expressed as

$$L = 11.93d^{0.398} \quad \text{trees in leaf (orchard)} \quad (1)$$

$$L = 8.02d^{0.368} \quad \text{conifer wood} \quad (2)$$

CONTENTS

(continued from front cover)

Low threshold optical differential amplification using a fibre amplifier in a nonlinear ring resonator F. J. Fraile-Pelaez, J. Capmany and M. A. Muriel (Spain)	page 1249	Applying two-stage photonic crossconnect to time-division multiplexed switch networks H. Obara and Y. Hamazumi (Japan)	page 1251
Novel optical circuit suitable for wavelength division bidirectional optical amplification S. Seikai, S. Shimokado and K. Kusunoki (Japan)	1268	OPTICAL FIBRES & SENSORS	
Novel technique for time resolving rare spectral events in DFB lasers D. J. Danagher, K. S. Visvanatha, R. Morris and R. Wilcox (Canada)	1296	In-line singlemode fibre interferometer via concatenated biconical tapers T. J. Brophy, L. C. Bobb and P. M. Shankar (USA)	1276
Refractive index step and optical confinement in $\text{Ga}_{0.86}\text{In}_{0.14}\text{As}_{0.13}\text{Sb}_{0.87}$/ $\text{Ga}_{0.73}\text{Al}_{0.27}\text{As}_{0.02}\text{Sb}_{0.98}$ double heterostructure lasers emitting at 2.2 μm M. S. S. Loral, M. B. Z. Morosini, J. L. Herrera-Perez, A. A. G. Von Zuben, A. C. F. da Silveira and N. B. Patel (Brazil)	1240	Mechanisms of enhanced UV photosensitivity via hydrogen loading in germanosilicate glasses R. M. Atkins, P. J. Lemaire, T. Erdogan and V. Mizrahi (USA)	1234
Singlemode surface emitting laser using partial mirror disordering T. G. Dziura, Y. J. Yang, R. Fernandez and S. C. Wang (USA)	1236	Overcoming the effects of polishing induced stress when fabricating fused polished couplers C. V. Cryan, J. M. Lonergan and C. D. Hussey (Ireland)	1243
MICROWAVE MEASUREMENTS & TECHNIQUES		Viscosity of F and GeO_2 codoped silica glass K. Shiraki, M. Ohashi, K. Tajima, M. Tateda and K. Tsujikawa (Japan)	1263
Attenuation functions of microwave signals propagated through trees M. O. Al-Nuaimi and A. M. Hammoudeh (UK)	1307	OPTICS	
Reduction of measurement error in microwave reflectometers by minimum sensitivity calibration J. Ladvánszky, A. Hilt and I. Csonka (Hungary)	1305	Enhanced single photon fringe visibility in a 10 km long prototype quantum cryptography channel P. D. Townsend, J. G. Rarity and P. R. Tapster (UK)	1291
Plane wave injection to calculate RCS in a 2-D TLM network J. B. Erwin and S. M. Wentworth (USA)	1241	OPTOELECTRONICS	
NEURAL NETWORKS		Multikilohertz all-optical modulator in semiconductor doped glass channel waveguide A. S. L. Gomes, Cid B. de Araujo (Brazil), A. Miliou and R. Srivastava (USA)	1246
Acceleration of backpropagation learning using optimised learning rate and momentum X.-H. Yu, G.-A. Chen and S.-X. Cheng (China)	1288	Proposal for ultra-compact electron transfer modulator structure Jin Wang, J. P. Leburton and J. E. Zucker (USA)	1293
Min-net winner-take-all CMOS implementation Y. He and E. Sánchez-Sinencio (USA)	1237	Resonant tunnelling light-emitting diode as optical switch S. Raymond, C. Van Hoof, J. Genoe, R. Mertens, G. Borghs, Z. Yan and E. Goovaerts (Belgium)	1301
Multiplierless multilayer feedforward neural network design suitable for continuous input-output mapping H. K. Kwan and C. Z. Tang (Canada)	1259	+20 dBm output power balanced optical amplifier module J.-M. P. Delavaux, Y. K. Park, K. A. Yanusheski, C. D. Chen, T. C. Pleiss, D. J. DiGiovanni (USA) and P. Martin (France)	1248
Very efficient VLSI implementation of CNN with discrete templates G. C. Cardarilli and F. Sargeni (Italy)	1286	SEMICONDUCTOR DEVICES & MATERIALS	
OPTICAL COMMUNICATIONS		P-type InP grown at low temperatures by atomic layer molecular beam epitaxy (ALMBE) M. I. Dotor, P. Huertas, P. A. Postigo, D. Golmayo and F. Briones (Spain)	1270
1.7 Gbit/s transmission over 217 km using a 16 x 1 photonic integrated circuit transmitter G. Raybon, U. Koren, M. G. Young, M. A. Newkirk, P. B. Hansen, B. I. Miller, M. Chien, M. Zirngibl, C. Dragone, B. Tell, H. M. Presby and C. A. Burrus (USA)	1295	Reduced indium incorporation during MBE growth of In(Al, Ga)As M. McElhinney and C. R. Stanley (UK)	1302
All-optical nonblocking $M \times M$ switchless connector with $O(\sqrt{M} \log M)$ wavelengths and without wavelength changers R. A. Barry (USA)	1252	Errata	1310